Numerical Simulation and Wind Tunnel Test Validation of the Aerodynamic Brake Panel

Liqiang Gao, Xiong Hu, Dejian Sun, Ying Xi and Guohua Wang

Abstract By means of numerical simulation and wind tunnel test to the simplified model of high-speed train with brake panels, the calculation precision was evaluated in simulating the external flow fields around the train with brake panels. In addition, three cases were researched, in which the running speed of the train is 150, 200 and 250 km/h respectively. Furthermore, multi-condition contrast were completed through numerical simulation and wind tunnel test, while the pressure distribution on the windward side of the brake panel and the aerodynamic resistance of the brake panel in wind direction were contrastively analyzed. Conclusions can be summarized from the results: The deviation of the aerodynamic resistance force is under 2% between simulation and test; the pressure distribution on the windward side of the brake panel is uniform, and the pressure difference at the geometrical center point is under 10% between simulation and test; so the numerical simulation to the external flow fields around the train with brake panels is also a reliable method other than wind tunnel test.

Keywords Aerodynamic brake · Brake panel · Wind tunnel test
Numerical simulation

1 Introduction

The quick transformation of kinetic energy is required when high-speed train is braking. While only some risky methods such as reducing braking speed as well as increasing braking time, the unsafe braking way etc. can be used based on traditional friction braking, because the heat capacity of brake disk can't bear the energy

L. Gao (✉) · X. Hu · D. Sun
College of Logistics Engineering, Shanghai Maritime University,
Shanghai 201306, China
e-mail: glq3318918@163.com

Y. Xi · G. Wang
School of Mechanical Engineering, Tongji University, Shanghai 201804, China

transformation from a train with a braking speed more than 300 km/h. Meanwhile, high-speed railway has developed rapidly in recent years in our country and a series of special lines for high-speed passenger trains like Beijing-Shanghai high-speed railway have come into service. Therefore, It's highly important that researching and developing some new non-adhesion braking methods which can also be utilized to high-speed trains as complement [1, 2]. The non-adhesion braking methods widely used in Europe are magnetic track or eddy current while aerodynamic brake is applied for both Maglev and Bullet Train in Japan. In both eddy current braking and magnetic track, additional braking device has to be installed under the bogie, which will not only add weight to the train but also bring track abrasion and magnetic radiation. On the contrary, aerodynamic brake is that unfolding brake panels on top of the train to gain more brake force by increasing air resistance. And the air resistance is in proportion to the square of velocity, which means a larger brake force can be achieved if the speed is higher. All in all, aerodynamic brake is significantly environmental-friendly, by taking good advantage of this kind of clean and natural energy [3].

Earlier research on aerodynamic brake were conducted in Japan [4, 5], but few documents are available. In China, Miao Xiu-juan from Central South University did some research on numerical simulation of brake panel [6], illustrated that a single brake panel can provide quite large force as a complemental device. Resistance pressure distribution in two cases that brake panels are installed on top of every carriage or not are analyzed in document [7]. However, no test results support these research, the reliability and calculation precision of numerical simulation for the external flow fields around the train with brake panels are still uncertain.

Based on the existing research results, by means of numerical simulation and wind tunnel test to the simplified model of high-speed train with brake panels, the calculation precision of numerical simulation was evaluated in simulating the external flow fields around the train with brake panels in this paper. In addition, three cases were researched, in which the running speed of the train is 150, 200 and 250 km/h respectively. Furthermore, multi-condition contrast were completed through numerical simulation and wind tunnel test, while the pressure distribution on the windward side of the brake panel and the aerodynamic resistance of the brake panel in wind direction were contrastively analyzed. Finally, the reliability of numerical simulation was verified.

2　Principle of Aerodynamic Brake

Aerodynamic brake, as one of the non-adhesion braking methods, takes advantage of pressure difference between two sides of the brake panel to generate resistance by unfolding the brake panels upon the roof, refer to Fig. 1 for detail. When the train runs normally, the brake panels are part of the train roof, aligned with it; while the

Fig. 1 The principle of generating braking force by the brake panel
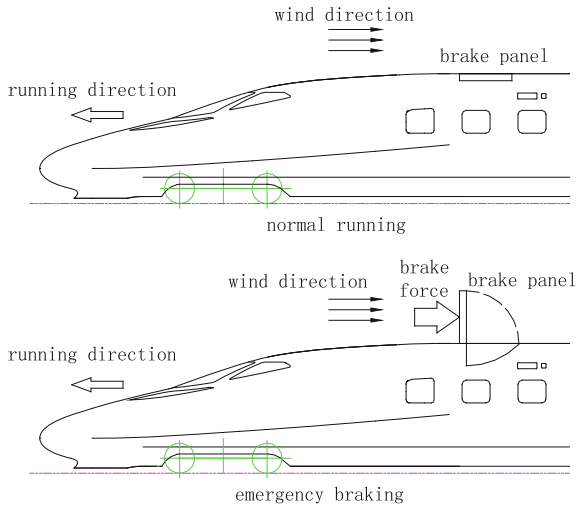
train needs emergency braking, the brake panels are raised by mechanical installations and act as braking components [4].

3 Numerical Simulation Calculation

3.1 Mathematical Model

When the train runs at high speed, complicated 3D turbulent flow will be generated around the train. In this paper, the turbulence was simplified as a mathematical model combining 3D transient N-S equation and k-ε equation. Then the external flow fields around the train can be numerically simulated with CFD software FLUENT. Besides, the finite volume method was used to discretize and solve the control equation. Furthermore, SIMPLE method was also considered to couple the pressure and velocity fields to find the numeric solution.

The equation of continuity can be expressed as

$$\frac{\partial \rho}{\partial t} + \frac{\partial(\rho u)}{\partial x} + \frac{\partial(\rho v)}{\partial y} + \frac{\partial(\rho w)}{\partial z} = 0 \tag{1}$$

The equations of momentum are

$$\frac{\partial(\rho u)}{\partial t} + \mathrm{div}(\rho u \bar{u}) = \mathrm{div}(\mu \, \mathrm{grad} \, u) - \frac{\partial p}{\partial x} + S_u \tag{2}$$

$$\frac{\partial(\rho v)}{\partial t} + \text{div}(\rho v \bar{u}) = \text{div}(\mu \text{ grad } v) - \frac{\partial p}{\partial y} + S_v \tag{3}$$

$$\frac{\partial(\rho w)}{\partial t} + \text{div}(\rho w \bar{u}) = \text{div}(\mu \text{ grad } w) - \frac{\partial p}{\partial z} + S_w \tag{4}$$

Equations (2), (3) and (4) make up the conservation equations of momentum, which are also named Navier-Stokes equations.

The equation of energy can be expressed as

$$\frac{\partial(\rho T)}{\partial t} + \text{div}(\rho \bar{u} T) = \text{div}\left(\frac{\kappa}{c_p} \text{grad } T\right) + S_T \tag{5}$$

The transport equation about the turbulent dissipation rate ε and turbulent kinetic energy k can be expressed as below

$$\frac{\partial(\rho k)}{\partial t} + \frac{\partial(\rho k \mu_i)}{\partial x_i} = \frac{\partial}{\partial x_j}\left[\left(\mu + \frac{\mu_t}{\sigma_k}\right)\frac{\partial k}{\partial x_i}\right] + G_k - \rho \varepsilon \tag{6}$$

$$\frac{\partial(\rho \varepsilon)}{\partial t} + \frac{\partial(\rho \varepsilon \mu_i)}{\partial x_i} = \frac{\partial}{\partial x_j}\left[\left(\mu + \frac{\mu_t}{\sigma_\varepsilon}\right)\frac{\partial \varepsilon}{\partial x_i}\right]$$
$$+ \rho C_1 E \varepsilon - \rho C_2 \frac{\varepsilon^2}{k + \sqrt{v\varepsilon}} \tag{7}$$

Here ρ is the density; t is the time; u, v, w are the components of the velocity vector $\bar{u}$ in the direction of x, y, z axis respectively; S_u, S_v, S_w are the generalized source items of the conservation equations of momentum; c_p is the specific heat; T is the temperature; κ is the fluid heat transfer coefficient; S_T is the viscosity-damping item; k is the turbulence kinetic energy; μ_t is the turbulent viscosity; σ_k is the Prandtl constant corresponding to the turbulence kinetic energy k; G_k is generation item of the turbulence kinetic energy k caused by the average velocity gradient; ε is the turbulent dissipation rate; σ_ε is the Prandtl constant corresponding to the dissipation rate ε; C_1, C_2 are the model constants; E is the time-averaged strain rate.

The simultaneous equations composed of the k-ε two-equation and the preceding time-averaged Eqs. (1)–(6) constitute the closed equations to solve the turbulent flow fields around the train.

3.2 Simulation Model

Taking a CRH high-speed train as reference, the simplified simulation model was built based on the wind tunnel test model with 3D software CATIA at a ratio 1:1

Fig. 2 Schematic diagram of
the simulation model
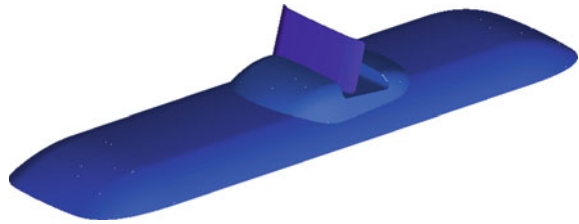
and consists of the train roof, the guiding shade and the brake panel. The train body
is 10 m long, and the model is shown in Fig. 2.

3.3 The Set of Computational Domain

Considering the influence of the ambient flows, both the inlet and the outlet should
be far away from the train to ensure uniform air flow velocity distribution, and the
distance should be more than three times of the train height [8, 9, 10]. 10 times was
chosen in this paper to ensure full development of the flow fields in this compu-
tational domain. The detailed set of the computational domain's spatial size is
shown in Fig. 3.

3.4 Boundary Conditions

The inlet is set as pressure-inlet boundary condition as in Fig. 3 and the calculation
formula of the total inlet pressure can be expressed as

$$\frac{p_0' + p_{op}}{p_s' + p_{op}} = \left(1 + \frac{\gamma - 1}{2} \mathrm{Ma}^2\right)^{\frac{\gamma}{\gamma - 1}} \tag{8}$$

Fig. 3 The set of
computational domain and
boundary conditions (unit: m)
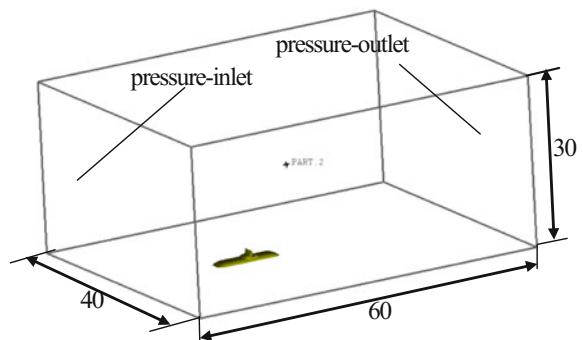
Here γ is the ratio of specific heat, and the value is 1.4 for air; Ma is the Mach number; $p_0{}'$ is the total inlet pressure; p_{op} is the operating inlet pressure, and the value in ground flow fields is 101,325 Pa; $p_s{}'$ is the static inlet pressure, and default value is 0.

The outlet is set as pressure-outlet boundary condition; ground is set as slip wall boundary condition, whose velocity is the same with the air flow; the surfaces of the train body and the guiding shade, the brake panel are set as non-slip wall boundary condition; the top and side faces of the air domain are set as non-slip smooth wall boundary condition.

3.5 Mesh Setting

The set of mesh is illustrated in Fig. 4. Non-structural mesh was used, Triangular Mesh for the surfaces of the brake panel, the train and Quad Mesh for the body. To ensure the accuracy of meshing, boundary layer control, mesh control and refining mesh have been done with the surfaces of the brake panel and the train. There are about 1.8 million body meshes in all calculating cases.

4 Wind Tunnel Test

Wind Tunnel, as a key device in train aerodynamic performance tests and researches, plays a very important role in high-speed train research and development. Compared with real train tests, wind tunnel test has some shining points such as low cost, good repeatability, controllability of test conditions and so on [11−12]. Tests in this paper were conducted in Aerodynamic-Aeroacoustic Wind Tunnel of Shanghai Ground Transportation Wind Tunnel Test Center in Tongji University. The size of the wind tunnel test section is 27 m × 17 m × 12 m, and the spout area is 7 m². Wind tunnel test section and the model of the high-speed train with brake panels can be found in Fig. 5. Due to the limitation of the test wind speed— 250 km/h in this Wind Tunnel Test Center, only three cases were researched with the wind speed as 150, 200 and 250 km/h respectively.

Six component balance measurement system was utilized to measure the aerodynamic resistance force to the brake panel in the air flow direction. To avoid vibration, the model of high-speed train was rigidly connected with the balance lever. In order to get the pressure distribution on the windward side of the brake

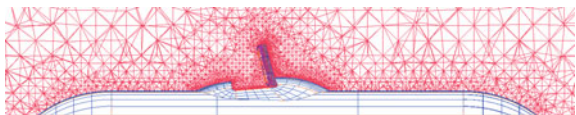**Fig. 4** The meshing around the brake panel and the train

Fig. 5 Wind tunnel test
section and the model of
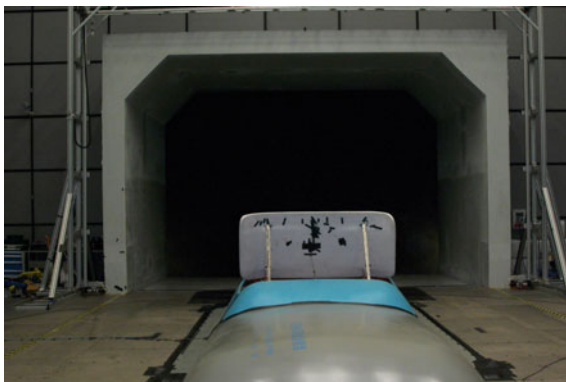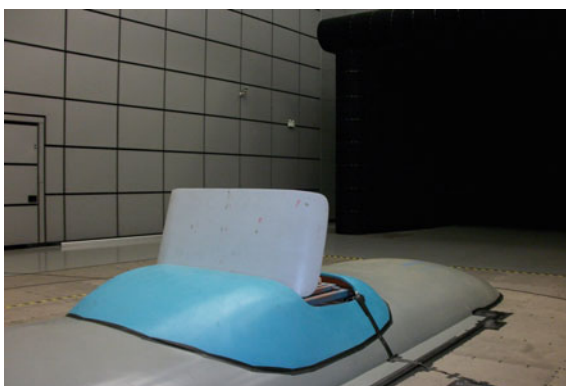high-speed train with brake
panels

Fig. 6 Wind tunnel test
section and the windward side
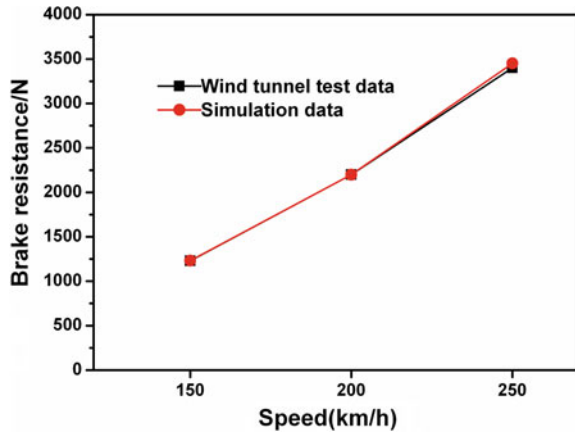of the brake panel

panel, small holes were punched at the test points of the panel and some pressure
sensors were put at the corresponding positions on the windward side through those
holes, measuring the pressure from the air flow, refer to Figs. 5 and 6. In this paper,
test result of the geometrical center point on the windward side of the brake panel
was taken to verify the outcome of numerical simulation.

5 Result Comparison Between Wind Tunnel Test and Numerical Simulation

5.1 Comparison of Aerodynamic Resistance Force

In the three compared cases, the wind speed is 150, 200 and 250 km/h respectively.
As shown in Fig. 7, for aerodynamic resistance force, the results are almost the same
between numerical simulation and tunnel test, with the largest deviation less than 2%.

Fig. 7 The comparison of aerodynamic resistance force


5.2 Comparison of Pressure Distribution on the Windward Side of the Brake Panel

In the three compared cases, the wind speed is 150, 200 and 250 km/h respectively. Same test point was chosen for both numerical simulation and wind tunnel test, it's at the geometrical center point. The comparison can be found in Table 1, and the results are not much far away from each other, with the largest deviation less than 10%, which can verify the reliability of numerical simulation.
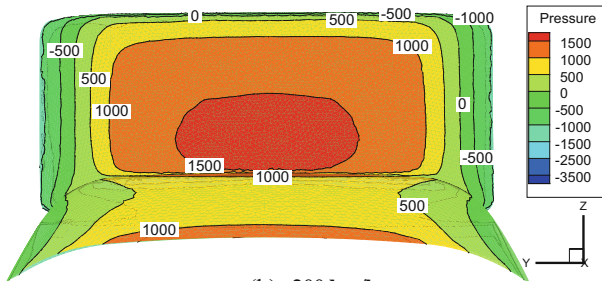
From Fig. 8, in numerical simulation, pressure distribution on the windward side is quite uniform and the pressure value in the central area is close to the value of test point.

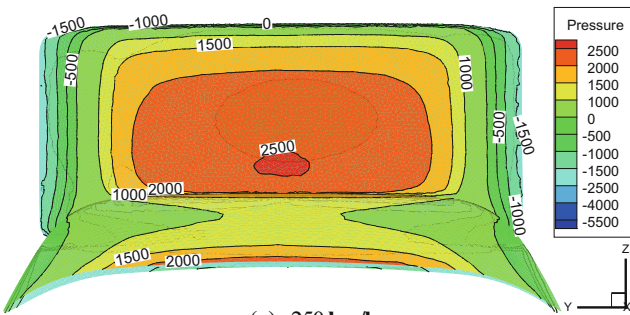**Table1** The comparison of the pressure at the test point

Wind speed (km/h)	Simulation (Pa)	Test (Pa)	Deviation (%)
150	896	970	7.6
200	1602	1706	6.1
250	2517	2693	6.5
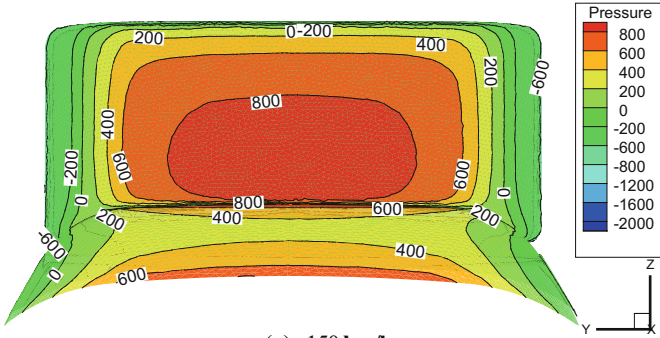
(a) 150 **km/h**

(b) 200 **km/h**

(c) 250 **km/h**

Fig. 8 The pressure distribution of the brake panel with different wind speed (unit: Pa)

6   Conclusions

(1) In three cases, the aerodynamic resistance force in both numerical simulation and wind tunnel test are almost the same, with deviation less than 2%.
(2) In three cases, the pressure distribution on the windward side of the brake panel is quite uniform; compared to the test result, the pressure at the geometrical center point on the windward side has a deviation less than 10%.
(3) The reliability and calculation precision of numerical simulation with k-ε two-equation turbulence model for the external flow fields around the high-speed train with brake panels can be verified by the above conclusions.

References

1. Albertz D, Dappen S. Calculation of the 3D non-linear eddy current field in moving conductors and its application to braking systems. IEEE Trans Magn. 1996;32(3):768–71.
2. Briginshaw D. The new generation of high speed train AGV in france. IRJ. 2000;40(5):15–8.
3. Zhou W. Japan's latest "sister" high—speed train-Fastech 360S type and Fastech 360Z high-speed train. Railway Knowl. 2006;1(4):17–17.
4. Masafumi Y. Characteristics of the aerodynamic brake of the vehicle on the Yamanashi maglev test Line. RTRI. 2000;41(2):74–8.
5. Kazumasa O, Masafumi Y. Development of aerodynamic brake of maglev vehicle for emergency use. RTRI. 1989;3(11):53–53.
6. Miao X-J, Liang X-F. Research on air brake board of high-speed Train. 04 Industrial aerodynamics conference. Beijing: Industrial Aerodynamics Conference, 2004:7–41.
7. Tian C, Wu M-L, Fei W-W. Rule of aerodynamics braking force in longitudinal different position of high- speed train. J Tongji Univ (Nat Sci). 2011;39(5):705–9.
8. Zhang J-H, Wang Ji-Q, Wu X-D. The numerical simulation of the turbulent characteristics of high-speed train. Rolling Stock. 2010;30(1):11–5.
9. Wang D-P. Technology research of creating CFD models and its verification in high speed train. Dalian, China: Dalian Jiaotong University; 2006. p. 87–8.
10. Wang F-J. Computational fluid dynamics (CFD software analysis principle and application. Beijing, China: Tsinghua University Press; 2004. p. 4–158.
11. Jing MA, Yang Z-G. Method of selecting high-speed train scale model for wind tunnel testing of aerodynamic drag based on numerical computation. Comput Aided Eng. 2007;16(3):110–3.
12. Xia C, Shan X-Z, Yang Z-G et al. A comparative study of different turbulence models in computation of flow around simplified train. J Tongji Univ (Nat Sci). 2014;42(11):1687–92.

Author Biography

Liqiang Gao born in 1986, is currently a postdoctor candidate at Shanghai Maritime University. He received his doctor degree from Tongji University, China, in 2017. His research interests include machine design theory and fluid dynamics.